Estimation of facies probabilities on the Snorre field using geostatistical AVA inversion

Sebastian Ng, StatoilHydro Research Center
Pål Dahle, Ragnar Hauge, Odd Kolbjørsen, Norwegian Computing Center

SUMMARY

We have done a geostatistical inversion of seismic data to facies probabilities. As a first step, we invert the seismic data for elastic parameters using the Bayesian AVA inversion method of Buland *et. al.* (2003). Next, we use an analysis of the uncertainty in the posterior distribution to filter the elastic parameters given in well logs. By comparing these filtered well logs with facies logs, we establish a relationship between facies and seismic data. This relationship is combined with the elastic parameters from the inversion to estimate facies probabilities for the entire volume.

INTRODUCTION

Seismic inversion is commonly done to obtain elastic parameters. This is natural, since the seismic response is defined by these parameters. However, they are useful only through their relation to reservoir parameters, such as porosity, fluid or facies. In this paper, we use the the Bayesian linearized AVA inversion method by Buland et. al. (2003) to obtain a distribution for the elastic parameters. Based on well logs, this distribution is then mapped to facies probabilities.

In the Bayesian inversion method, the earth model $(\ln V_p, \ln Vs, \ln \rho)$ is given by a multi-normal distribution with spatial coupling imposed by correlation functions. A prior model for the earth model is set up based on well logs. Linearization of the relationship between the earth model parameters and the seismic data allows analytical computation of the posterior distribution. Facies probability volumes are obtained from the posterior distribution using relationships between elastic parameters and facies obtained from well logs. From the stochastic inversion, we have the uncertainty of the inverted parameters, and use this when computing the probabilities. The result is facies probability cubes, intended for use in lithology prediction and geomodeling.

A classic problem when predicting facies from elastic parameters obtained by seismic inversion is how to associate facies and elastic parameters. One approach is to sample the inversion into the well, and associate facies and inverted values. But since the well logs are in depth and the inversion is in time, time to depth conversion errors will have large influence here. Another approach is to use frequency-filtered well logs of the elastic parameters, and assume that these are representative for the inversion, but this will tend to be too optimistic. Our approach is to use a filter obtained from the seismic inversion, which defines what information the inversion has captured. This gives accurate probabilities from the inversion, provided the well-tie is good.

We have used this approach on the Snorre field (see Figure 1). The Snorre field, which was proven in 1979, is about 191km^2
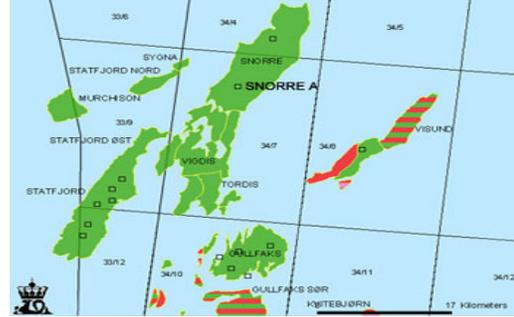

Figure 1: The Snorre Field and its neighbor fields. [Ref.: NPD - Norwegian Petroleum Directorate]

in extent and located in the Tampen area in the northern North Sea. The reservoir section, more than 1000m thick, consists of complex submarine-fluvial channel systems with sequences of sandstone and shale at depths of 2.5 km, mainly terrestrial deposits. Individual sandstones and shales are relatively thin compared to the seismic resolution. The rotated structure combined with later uplift results in several tilted fault blocks.

THEORY

Bayesian inversion

We have treated the earth as an isotropic, elastic medium. Such a medium can be modeled by the elastic parameters, which depend on the lateral position and vertical seismic travel time only. The inversion method uses the weak contrast approximation of the PP reflection coefficient by Aki and Richards (1980)), in which we replace the V_s/V_p ratio, wherever present, by a constant. The seismic data is modeled as the convolution of the wavelet with the reflectivity coefficient plus an error term. After discretization the earth model reads

$$\mathbf{m} = \left[\ln \mathbf{V}_p, \ln \mathbf{V}_s, \ln \boldsymbol{\rho}\right]^T. \qquad (1)$$

where $\mathbf{V}_p$ is the pressure-wave velocity, $\mathbf{V}_s$ is the share-wave velocity, and $\boldsymbol{\rho}$ is the density. With the assumptions given above the seismic data becomes

$$\mathbf{d} = \mathbf{Gm} + \mathbf{e}, \qquad (2)$$

where $\mathbf{d}$ are the seismic data, $\mathbf{m}$ is the earth model and $\mathbf{e}$ is the noise. The matrix $\mathbf{G}$ contains both the convolution and the transformation from earth model to reflectivity coefficients. The wavelet depends on the angle and is assumed to be stationary within a certain limited target window.

Using multi-normal distributions, the earth model $\mathbf{m}$ and error $\mathbf{e}$ can be written as

$$\mathbf{m} \sim \mathcal{N}\left(\boldsymbol{\mu}_m, \Sigma_m\right) \qquad (3a)$$
$$\mathbf{e} \sim \mathcal{N}\left(\mathbf{0}, \Sigma_e\right), \qquad (3b)$$

where $\boldsymbol{\mu}_m$ is the expectation vectors of the logarithm of the elastic parameters, and Σ_m is their covariance. The expectation vectors are normally referred to as the background model. For the error model we use zero-mean Gaussian noise which is assumed independent of $\mathbf{m}$. The error covariance Σ_e consists of both a white noise part and a coherent noise part.

From Eq. 2, the seismic data are linked to the earth and error models through linear operations only. Hence, the seismic data will also be multi-normal, that is, $\mathbf{d} \sim \mathcal{N}(\mu_d, \Sigma_d)$. This implies that the simultaneous distribution for both $\mathbf{m}$ and $\mathbf{d}$ is multi-normal, and the posterior distribution for $\mathbf{m}$ given $\mathbf{d}$ can be obtained, straight-forwardly, as

$$\boldsymbol{\mu}_{m|d_{\text{obs}}} = \boldsymbol{\mu}_m + \Sigma_{d,m}^T \Sigma_d^{-1}(\mathbf{d}_{\text{obs}} - \boldsymbol{\mu}_d) \qquad (4a)$$

$$\Sigma_{m|d_{\text{obs}}} = \Sigma_m - \Sigma_{d,m}^T \Sigma_d^{-1} \Sigma_{d,m}, \qquad (4b)$$

where $\Sigma_{d,m}$ is the cross-covariance between logarithmic parameters and observations. To avoid the time-consuming calculation of Σ_d^{-1}, Eqs. 4a and 4b are solved in the Fourier domain, by assuming that the seismic residuals are second-order stationary Gaussian fields (see Buland *et. al.* (2003)).

Facies prediction
To obtain facies probabilities, we use a point-wise approach where we predict the facies probability in one location from the inverted parameters in that location. The facies probability in spatial location $\mathbf{i} = (i_1, i_2, i_3)$ is given by a standard Bayesian updating,

$$\mathrm{P}(f_{\mathbf{i}} = k|\hat{\mathbf{m}}_{\mathbf{i}}) = \frac{p(\hat{\mathbf{m}}_{\mathbf{i}}|f_{\mathbf{i}} = k) \cdot p(f_{\mathbf{i}} = k)}{\sum_j p(\hat{\mathbf{m}}_{\mathbf{i}}|f_{\mathbf{i}} = j) \cdot p(f_{\mathbf{i}} = j)}, \qquad (5)$$

where $p(f_{\mathbf{i}} = k)$ is the prior probability for a facies k in location $\mathbf{i}$, and $p(\hat{\mathbf{m}}_{\mathbf{i}}|f_{\mathbf{i}} = k)$ is the distribution for the inverted elastic parameter given facies k in location $\mathbf{i}$.

In this presentation we use a constant prior probability, that is, $p(f_{\mathbf{i}} = k) = p_k^0$, but this could easily be substituted with a spatially varying probability. The constant prior probability is obtained from the well logs in the region in study.

In our approach, we model the distribution of facies relative to the background model $\boldsymbol{\mu}_{\mathbf{m},\mathbf{i}}$, that is

$$p(\hat{\mathbf{m}}_{\mathbf{i}}|f_{\mathbf{i}} = k) = g_k(\hat{\mathbf{m}}_{\mathbf{i}} - \boldsymbol{\mu}_{\mathbf{m},\mathbf{i}}) \qquad (6)$$

This means that the distribution of inversion parameter for a given facies has the same shape in all spatial locations, but it is shifted relative to a background model. The distributions g_k are not known and must be estimated. We estimate these from filtered well logs. We extract all values that correspond to a given facies from the filtered well logs, and use 3D kernel estimation to obtain an approximation of the density.

The filter $\mathbf{F}$ that is applied to the well logs is computed based on the difference in the prior and posterior covariances. This filter defines the information content the inversion has captured, and is defined such that the frequency content in the filtered well logs is equal to that of the inverted parameters. Formally, this may we written

$$\hat{\mathbf{m}} = \mathbf{Fm}. \qquad (7)$$

Note that the filter is applied to all three parameters in the well logs simultaneously such that it also captures the interactions of the parameters in the estimation.

THE TEST CASE

Prior model
The prior model for the inversion consists of the expectation values $\boldsymbol{\mu}_m$ and the covariance Σ_m. The expectation values constitute the background model for the inversion. The background model was obtained from well logs by filtering elastic parameter raw logs to high-cut frequency 6 Hz. From these filtered logs we estimated a vertical trend and added local variation correction around each well using kriging. For the kriging we used an isotropic, exponential correlation function with a range of 3.5km in the north-west to south-east direction and a range of 2.5km perpendicular to this.

The prior covariance was decomposed into a 3×3 parameter covariance matrix that was estimated from wells logs, a parametric, lateral correlation function with ranges 800m and 400m and the same anisotropy angle as above, and a temporal correlation function estimated from well logs.

For the likelihood, the covariance was decomposed similarly. The covariance matrix was constructed using signal-to-noise ratios obtained during the wavelet estimation, the lateral correlation was set equal to that of the prior model, and the temporal correlation was computed from the wavelet. To allow errors on all frequencies, 10% white noise was added.

Wavelet estimation
The wavelets, which are displayed in Figure 2, were estimated independently for each angle using a standard tapering approach (see White (1984)). Wavelet estimates from different wells were peak aligned and a common scale was selected to minimize the residuals. In order to enhance the visibility of the
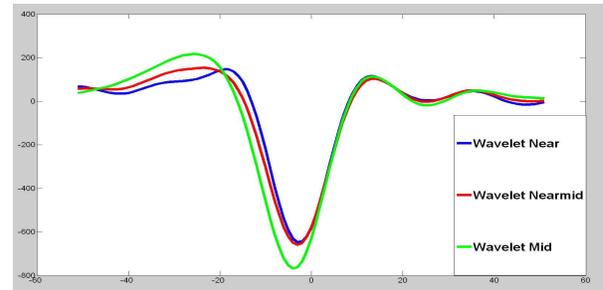

Figure 2: The estimated wavelet for different angular stacks.

area of interest, the wavelets were estimated using the reservoir interval only, with a taper zone slightly above and below.

INVERSION RESULTS

The inversion interval was defined by two smoothed, interpreted surfaces, taken to represent the major correlation directions in the reservoir structure. The inversion grid had a

lateral resolution of $25m \times 25m$ and a sampling density better than 4.0ms. For the inversion grid this amounted to 230 million grid cells, and the complete facies probability estimation required some 40 minutes using a modern Linux PC. This inversion employed three AVA stacks (near, near-mid and mid) and six vertical wells.
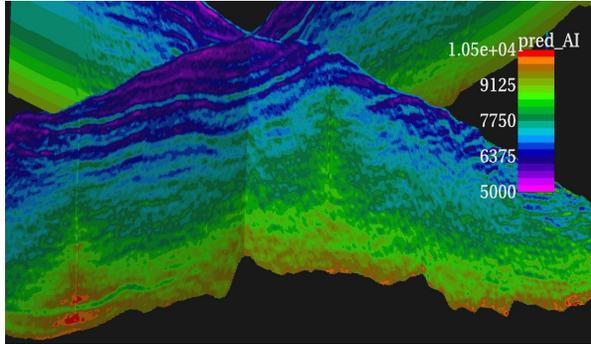

Figure 3: Cross sections of the predicted AI. Also shown are two AI well logs filtered to 40 Hz.
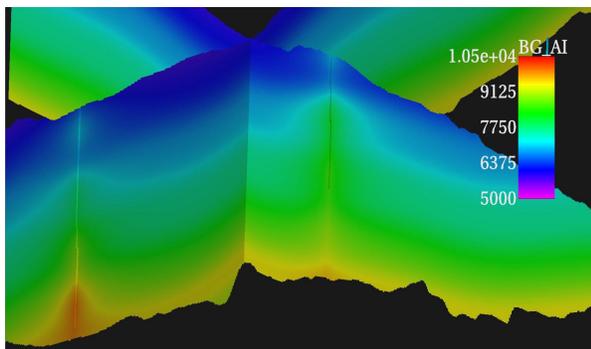

Figure 4: The background model for AI. Also shown are two AI well logs filtered to 6 Hz.

In Figure 3, we show a cross section of the acoustic impedance (AI). Also shown are two 40 Hz high-cut filtered AI well logs. The prediction shows good agreement with the well logs. For comparison, the background model for AI is given in Figure 4. For the background we have used a continuous color scale to maintain the smoothness in the plot.

Facies probabilities

In Figure 5, we have given a facies log for one well with the probability for sand calculated both with and without this well. This blind test shows that we are able to predict the major sands and shales, but also that there are some alignment problems in the center part of the log.

To identify the amount of facies information that may be extracted from the seismic data, we have plotted AI vs. V_p/V_s ratio for raw logs (Figure 6) and logs filtered to seismic resolution (Figure 7). In both cases we use the resolution of the inversion grid and give the axes in logarithmic scale and relative to the background. The plot with raw logs shows that
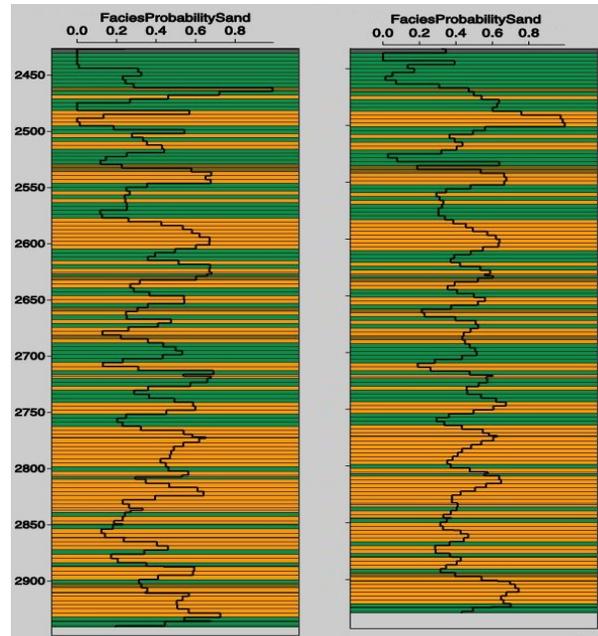

Figure 5: Probability of sand (black curve) against facies in well log (green=shale, orange=sand, brown=crevasse). The shown facies log was included in the calculation of facies probabilities for the right plot but was excluded for the left.
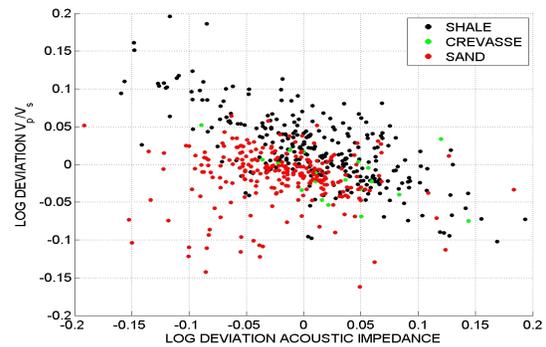

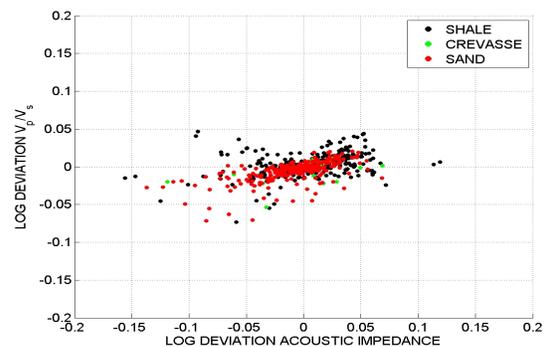Figure 6: Cross plots of AI versus V_p/V_s ratio from raw logs.

Figure 7: Cross plots of AI versus of V_p/V_s ratio from logs filtered to seismic resolution.

shale and sand are fairly well separated whereas crevasse is not. When we compare this plot with the plot where the logs have been filtered to seismic resolution using Equation 7, we see that even with three AVA stacks, the inversion does not give much information about the V_p/V_s ratio. This means that the facies prediction must be done mainly on acoustic impedance.

In order to check the quality of our result, we consider a prediction ability measure: We look at the average probabilities for facies in all cells that have the same facies in the well log. That is, we first run through all cells where the well log shows shale, and compute the average sand probability, crevasse probability and shale probability. This is repeated for the cells where the well shows crevasse, and finally for the sand cells. Perfect prediction would occur if the shale probability was 1 when true facies was shale, and so on.

The best prediction possible given the elastic parameter distribution seen in raw well logs is a useful reference level. These numbers are shown in Table 1.

Predicted	True facies		
facies	shale	crevasse	sand
shale	0.713	0.350	0.288
crevasse	0.028	0.095	0.045
sand	0.259	0.555	0.667

Table 1: Probability table constructed from raw well logs.

As we see, the probability for sand is high when the truth is sand or crevasse, and low when the truth is shale, whereas the opposite is true for shale. From this table, we see that we can not expect to get good probabilities for crevasse. The elastic parameters for crevasse is too close to sand, and there is much more sand than crevasse seen in the wells.

Predicted	True facies		
facies	shale	crevasse	sand
shale	0.589	0.496	0.439
crevasse	0.036	0.103	0.038
sand	0.374	0.401	0.522

Table 2: Probability table constructed from filtered well logs.

In Table 2, we have done the same computation, but with filtered well logs. This is what we can expect after inversion, and the prediction is clearly weaker than in Table 1. The main reason for this is that we after inversion have little useful information form the V_p/V_s ratio, as seen in Figures 6 and 7. The prediction is still much better than a flat prior, however, as the sand probability is 50% higher when the truth is sand compared to shale.

In Table 3 we have computed the same numbers using the actual inversion instead of well logs. We are now getting close to a flat distribution. In addition, there is now a small probability of undefined, which occurs when the elastic parameters from the inversion are outside the range spanned by the filtered well logs. The difference between Tables 2 and 3 is caused by both time to depth conversion error of well-log and model errors. The reservoir has thin facies intervals (see Figure 5) and

Predicted	True facies		
facies	shale	crevasse	sand
shale	0.511	0.482	0.505
crevasse	0.036	0.023	0.037
sand	0.407	0.443	0.435
undef	0.045	0.051	0.024

Table 3: Probability table constructed from inversion results.

is therefore sensitive to time to depth conversion errors when computing the performance statistics in Table 3. This type of error is not present in Table 1 and 2 since these only relate to well log data. This may explain part of the flattening of the distribution. A more detailed analysis of the well logs and inverted facies cube shows that the prediction is better than average in some zones. For example is the Dunlin formation seen as a diagonal red line between two purple lines at the top left in Figure 8 easy to identify. This might indicate that this is a region where the model of relative deviations is good. Generally better predictions can be obtained if more information regarding the relative behavior of sand and shale is used.
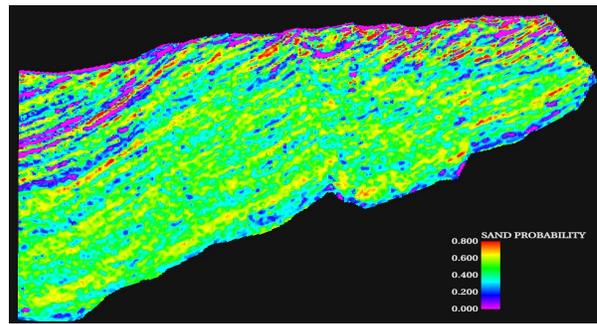

Figure 8: Cross section of the sand probability volume.

CONCLUDING REMARKS

We have shown how the Bayesian AVA inversion approach can be useful in order to obtain facies probabilities for geomodeling. In a complicated real world reservoir case, we see an increase of 50% in sand probability in the cells where well logs have sand compared to those with shale. A geomodel not using seismic data would have the same probability in both cases, so utilizing the seismic data in this way will have significant impact on the sand configuration. The algorithm presented is fast, and handles the uncertainty in the inversion correctly.

ACKNOWLEDGMENTS